Observations of the influence of turbulence on lightning initiation and propagation

Jessica Souza[1] and Eric Bruning[1]

[1]Texas Tech University

November 24, 2022

Abstract

The updraft speed is correlated to the total lightning flashes a storm produces. Shear along updraft gradients is one of the mechanisms responsible for the production of turbulence kinetic energy (TKE). Thus, the radar-estimated eddy dissipation rate (EDR) overlapped with Lightning Mapping Array (LMA) data is used to evaluate the storm's kinematic and electrical relationship. The majority of the flashes sampled shows highly turbulent regions involved in lightning initiation with more breakdown processes associated with smaller flashes. As the distance from flash initiation increases, there is a gradient to less turbulent regions favoring larger flashes propagation. We also identified small- and medium-sized flashes initiated at lower altitudes in regions of smaller EDR values, consistent with the unmixed flow within inner part of updrafts and a concentration of small flashes initiated in the upper portion of the cloud in high EDR values due to their associated small scale variability.

Observations of the influence of turbulence on lightning initiation and propagation

Jessica C. S. Souza[1], **Eric C. Bruning**[1]

[1]Department of Geosciences, Atmospheric Science Group, Texas Tech University, Lubbock, Texas, USA

Key Points:

- A gradient of small flash in highly turbulent regions to larger flashes in less turbulent regions is observed.
- The upper limit in turbulence intensity permitted for flash propagation in a region varied with the distance from flash initiation.
- A lower bound on turbulence intensity for flash initiation was not clear as small values close to initiation were noted in low altitudes.

Corresponding author: Jessica C. S. Souza, `jessica.souza@ttu.edu`

Abstract

The updraft speed is correlated to the total lightning flashes a storm produces. Shear along updraft gradients is one of the mechanisms responsible for the production of turbulence kinetic energy (TKE). Thus, the radar-estimated eddy dissipation rate (EDR) overlapped with Lightning Mapping Array (LMA) data is used to evaluate the storm's kinematic and electrical relationship. The majority of the flashes sampled shows highly turbulent regions involved in lightning initiation with more breakdown processes associated with smaller flashes. As the distance from flash initiation increases, there is a gradient to less turbulent regions favoring larger flashes propagation. We also identified small- and medium-sized flashes initiated at lower altitudes in regions of smaller EDR values, consistent with the unmixed flow within inner part of updrafts and a concentration of small flashes initiated in the upper portion of the cloud in high EDR values due to their associated small scale variability.

Plain Language Summary

The strength of the rising current within a thundercloud correlates with the intensity of turbulence production and the amount of lightning flash incidence. In this study, we evaluate the turbulence intensity in different parts along lightning flashes propagation. The results show that turbulence intensity is higher in locations closer to the lightning initiation and decreases as the distance from lightning initiation increases. However, there's also presence of lower intensity turbulence close to lightning initiation. Therefore, the results suggest a range of turbulence intensity favorable for lightning propagation and a minimum threshold for lightning initiation.

1 Introduction

Turbulence in thunderclouds acts on a continuum of scales (Bryan et al., 2003) and can be produced by distinct mechanisms. At large scales of about 10 km, turbulence production by buoyancy is responsible for the energy input in the system through thermals of up to 2 km in radius (Hernandez-Deckers & Sherwood, 2016) and their aggregation into the storm-scale updraft. In intermediate scales of tens of meters to a few km, turbulence is relevant for entrainment processes that may affect the vertical motion. On the smallest scales turbulence influences hydrometeor processes such as collision, coalescence and collection (Devenish et al., 2012). Characterizing the flow motion is intrinsically challenging due to the variety of instruments and methods required to account for processes acting across a large range of scales.

Turbulent convective motions occur simultaneously with the development of electric fields in thunderstorms, and their coupling has long been discussed (Colgate, 1967). Rebounding collisions between graupel particles and ice crystals with different masses and inertia is the main charge separation mechanism in thunderstorms, and is known as non-inductive relative-growth rate electrification mechanism (Saunders, 2008), which is determined by ambient temperature, cloud water content, rime accretion rate, and droplet size (Takahashi, 1978; Saunders & Brooks, 1992; Takahashi & Miyawaki, 2002). After sedimentation of the hydrometeors, a layered tripole model of charge distribution is expected (Williams et al., 1989). It contains an upper positive charge region of ice crystals, a main negative charge region of graupel and ice crystals, and a lower positive charge region of graupel. However, charge distributions are observed to become more complex than this in general (Stolzenburg et al., 1998; Bruning et al., 2010; Calhoun et al., 2013).

At large scales, the effectiveness of the non-inductive charging mechanism is supported by an updraft of about 5 m s^{-1} or more in the mixed phase region (0 °C to -40 °C) of the cloud (Deierling & Petersen, 2008). Deierling and Petersen (2008) established a correlation between total lightning activity and updraft volume for different storm types.

Higher updraft speeds were capable of producing more hydrometeors in the mixed phase region, and therefore more collisions, resulting in more charge separation and lightning flashes. Lund et al. (2009), Bruning et al. (2010), and Calhoun et al. (2013) for example, also observed that stronger updrafts produced more lightning discharges. Stolzenburg et al. (1998) showed through statistical investigation that the center height of the main negative charge region increased with increasing average balloon ascent rate and updraft speed in Mesoscale Convective Systems (MCS) and supercells.

Mareev and Dementyeva (2017) and Kostinskiy et al. (2020) approached lightning initiation by focusing on the influence of turbulence on small scales. In Mareev and Dementyeva (2017), the electric field growth and enhancement due to turbulence acting on the charge separation mechanisms in the electrification model relied on the hydrometeor-scale interactions. Its contribution could enhance the already built electric field locally and lead to lightning initiation. Kostinskiy et al. (2020) proposed a mechanism that allowed for lightning initiation considering the role of turbulence in creating numerous small high "electric field volumes" in a region of a thundercloud with background electric field comparable to values found in observations.

At the energy-containing end of the turbulence kinetic energy spectrum, updraft strength is connected to lightning activity and to eddy production. At the dissipative end, the influence of small eddies in hydrometeor interactions support electrification processes that clouds undergo, ultimately establishing preferred locations for lightning. Together, these relations also imply a plausible influence of turbulence on lightning in between these two ranges. In the inertial range (Kolmogorov, 1941), we expect the eddies to organize the net charge depending on the amount of energy received associated with the updraft strength.

Brothers et al. (2018) simulated, using a large-eddy-resolving model (125 m grid), the organization and evolution of different charging mechanisms that lead to the observed complexities in charge structure. Their results show that resolved turbulent eddies of the order of 1 - 2km in multicells were one of the most relevant mechanisms controlling the texture of the charge distribution in thunderclouds. Additionally, Bruning and MacGorman (2013) showed a relationship between flash area and flash rate matching the $-\frac{5}{3}$ slope predicted for turbulence kinetic energy in length scales of the inertial range in thunderstorms. This result led them to suggest a connection between the turbulence-driven eddies and the generation of electrical energy in the storm by convection. However, the lack of kinematic data for the storms analyzed prevented them from further exploring their hypothesis.

Combined kinematic and electrical observations are needed to assess the role turbulent, eddy-scale motions play in organizing charge. Consistent with prior studies, we hypothesize that turbulent regions favor more flash initiation and smaller lightning flashes, while less turbulence is found in regions of flash propagation. Prior studies did not address whether more extensive flashes are ever permitted in regions of greater turbulence, or if small flashes take place in regions of low turbulence. Thus, the goal of this study is to analyze observational data that supports the coupling between kinematic and electrical characteristics of storms in the inertial range that have not previously been well-observed, expanding the relationship proposed by Bruning and MacGorman (2013).

2 Data and Methodology

2.1 Data Set

The thunderstorms investigated are part of the Kinematic Texture and Lightning (KTaL) field experiment dataset (see supporting information for details). The KTaL experiment was designed to quantify eddy-scale kinematics and the distribution of energy in the convective flow while also characterising lightning discharges in different storm modes.

The intensive operational period occurred across the South Plains near Lubbock, TX during the spring and summer of 2014, 2015, and 2016 (Supporting information, Figure S1).

Continuous range-height indicator (RHI) scans of spectrum width, radial velocity, and radar reflectivity were collected every 10 s from 0.5° to 60° in elevation by the two Texas Tech University (TTU) mobile Ka-band radars (Hirth et al., 2012). Level-II reflectivity data collected at the KLBB (Lubbock, Texas) site of the Weather and Surveillance Radar - 1988 Doppler (WSR-88D) (Crum & Alberty, 1993) network was used to characterize where the TTU Ka-band radar measurements were taken relative to the storms.

Lightning data was collected by the West Texas Lightning Mapping Array (WTLMA) (Chmielewski & Bruning, 2016) that consists of 11 stations. The LMA is a system that detects the impulsive very high frequency (VHF) noise sources that are emitted by lightning during propagation. The VHF source points are then mapped into three spatial dimensions and time using time-of-arrival differences between the stations in the array, providing the lightning channel path to an accuracy of about 10 m above the network (Rison et al., 1999; Thomas, 2004).

2.2 Data Processing

The radar and LMA data were pre-processed before further analysis. First, the VHF sources were grouped into flashes by LMAtools. The temporal and spatial thresholds considered were the lmatools default of 0.15 s and 3 km, respectively, with a maximum duration of 3 s. Details of the flash sorting process are described in Fuchs et al. (2015). The flash initiation location (latitude, longitude, altitude) and flash area were also retrieved.

The radar data were processed and plotted using Py-ART (Python ARM Radar Toolkit) package (Helmus & Collis, 2016). We evaluated the turbulence intensity by the magnitude of the eddy dissipation rate (EDR) and the spatial velocity derivatives. EDR was estimated based on reflectivity and spectrum width measurements by applying the Python Turbulence Detection Algorithm (PyTDA) (Lang & Guy, 2017). PyTDA is a re-implementation of the National Center for Atmospheric Research (NCAR) Turbulence Detection Algorithm (NTDA) (Williams et al., 2006). In the EDR estimate, it is assumed that the radar illumination function is a 3D Gaussian, the reflectivity is uniform within the illumination volume, the energy spectrum presents an idealized shape, and turbulence is isotropic and homogeneous. The EDR estimate assumes an outer length scale of 500 m, and the turbulence kinetic energy spectra calculated from the radial velocities confirmed that an inertial range was present at length scales less than 500 m.

We calculated the spatial velocity gradient directly from the radial velocity at each range gate only in range and in elevation due to one azimuth restriction to provide information about the resolved velocity variability.

To compare the radar measurements in the radar coordinate system (elevation, azimuth, range) to lightning LMA data in the geographic coordinate system (longitude, latitude and altitude), we transformed their coordinates to the Rotated Tangent Plane Coordinate System. This results in the x-axis pointing into the direction of the radar fixed azimuth and values on the y-axis as orthogonal distance from the RHI scan (counterclockwise). Direct transformation of the data coordinates without an objective analysis or interpolation increases confidence in the alignment of the overlapping of lightning and radar data sets, and allows use of the raw data values.

2.3 Data Coupling

Each RHI scan from all storms (Supporting information, Table S1) was checked for at least one VHF source from a lightning flash during that scan. In that case, the

sources from the entire lightning flash were associated with that radar scan and checked for spatial proximity.

At least one VHF source had to be within 100 m of the RHI scan for that scan to be considered as intercepted by lightning. This threshold is related to the spatial scale of breakdown processes. Theoretically, Colgate (1967) demonstrated based on the Kolmogorov spectrum that the eddy size of 100 m is predicted for the initiation of lightning discharges because it has sufficient energy density to give a stress comparable to the electric field breakdown. In observations, the electric field magnitudes exceeded the runaway breakdown threshold for initiating lightning in volumes with a characteristic scale of 100m or less (Marshall, 2005). Moreover, Edens et al. (2014) showed that leader step lengths at mid-and upper-levels in thunderstorms were on the order of 100 m. 62.1 % of the lightning selected by this approach had a source within 20 m of the RHI plane which is less than the expected location error (spatial standard deviation of 34 m) within 50 km radius of the LMA Chmielewski and Bruning (2016).

The last requirement was that the intercepted location was in a region of good radar data quality. It was expected that more VHF sources would be present in more turbulent areas of the RHI scan. However, these regions can be challenging to sample since they often correspond to regions of hydrometeors that cause signal attenuation. The radar cone of silence also eliminated some regions of potential analysis. Thus, all RHI crossing points were inspected automatically and manually for consistency.

Then, independent of the minimum source orthogonal distance within the threshold, the next steps assumed it to be zero, i.e. laying on the RHI plane. This point of interception was transformed back to the radar coordinate system to identify the closest range gate. This Nearest Neighbor approach rely on the radar high resolution to produce an accurate estimate. However, estimates based on a single point can lead to an unrealistic analysis due to gate to gate variability. Distance-dependent weighted-average objective analysis was used to obtain the radar variables (spectrum width, radial velocity, EDR, and the radial velocity derivatives in space) for the point of interception. The euclidean distance between the flash initiation location and the point of interception was also stored. When there were more than one VHF source within the threshold, the final distance and radar variables values were calculated also as a weighted average. The weights followed a Gaussian function with $w(d = 0) = 1$ and $w(d = 100) = 10^{-2}$, where d is the distance from the RHI scan.

3 Results and Discussion

The methods identified 404 lightning flashes presented in figure 1. Figure 1 shows (a) EDR and (b) spatial velocity derivatives as a function of the distance between where the lightning flashes crossed the radar scans and each flash initiation.

In figure 1 (b), the velocity gradient in space had a zero mean and the similar symmetric distribution in the sampled locations for both terms is consistent with isotropy. The large spread observed in smaller flashes is associated with more variability in velocity distribution. The magnitude of the dispersion from the mean decreases from smaller to larger flash areas.

The survey of the patterns associated with flash initiation and propagation observed in figure 1 across each RHI scan analyzed allowed the identification of different behaviors (Figure 2 and 3). The groupings of data found were: a decrease in turbulence intensity with increasing distance from flash initiation; high turbulence intensity near flash initiation; and low turbulence intensity near flash initiation. There were no observations of high turbulence intensity far from flash initiation.

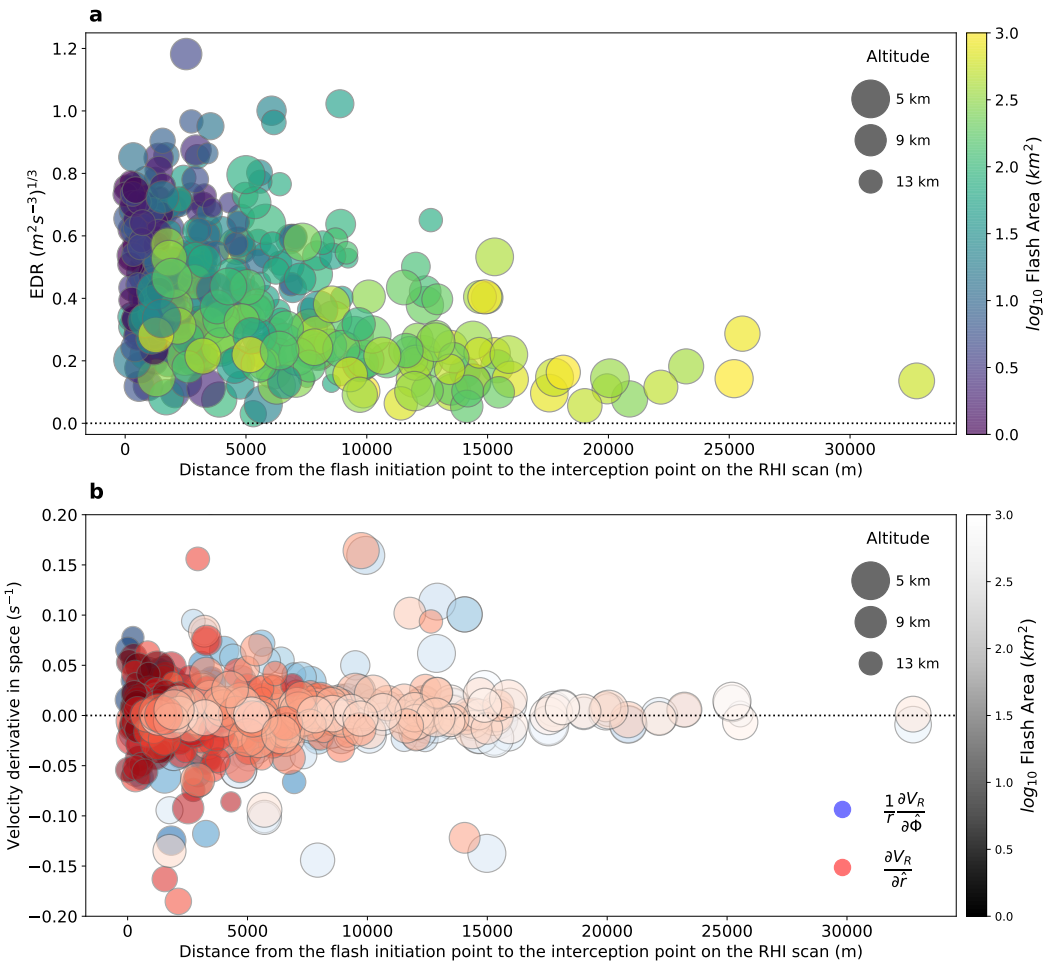

Figure 1. Radar-measured velocity characteristics for the 404 lightning flashes intersecting radar scans in the storms analyzed. Each point is colored by its area. Symbol size is proportional to the initiation altitude. (a) Spectrum width-estimated EDR and (b) radial velocity derivatives in space for the location intercepted by lightning as a function of the distance between the parent lightning initiation point and the point of interception on the RHI scan.

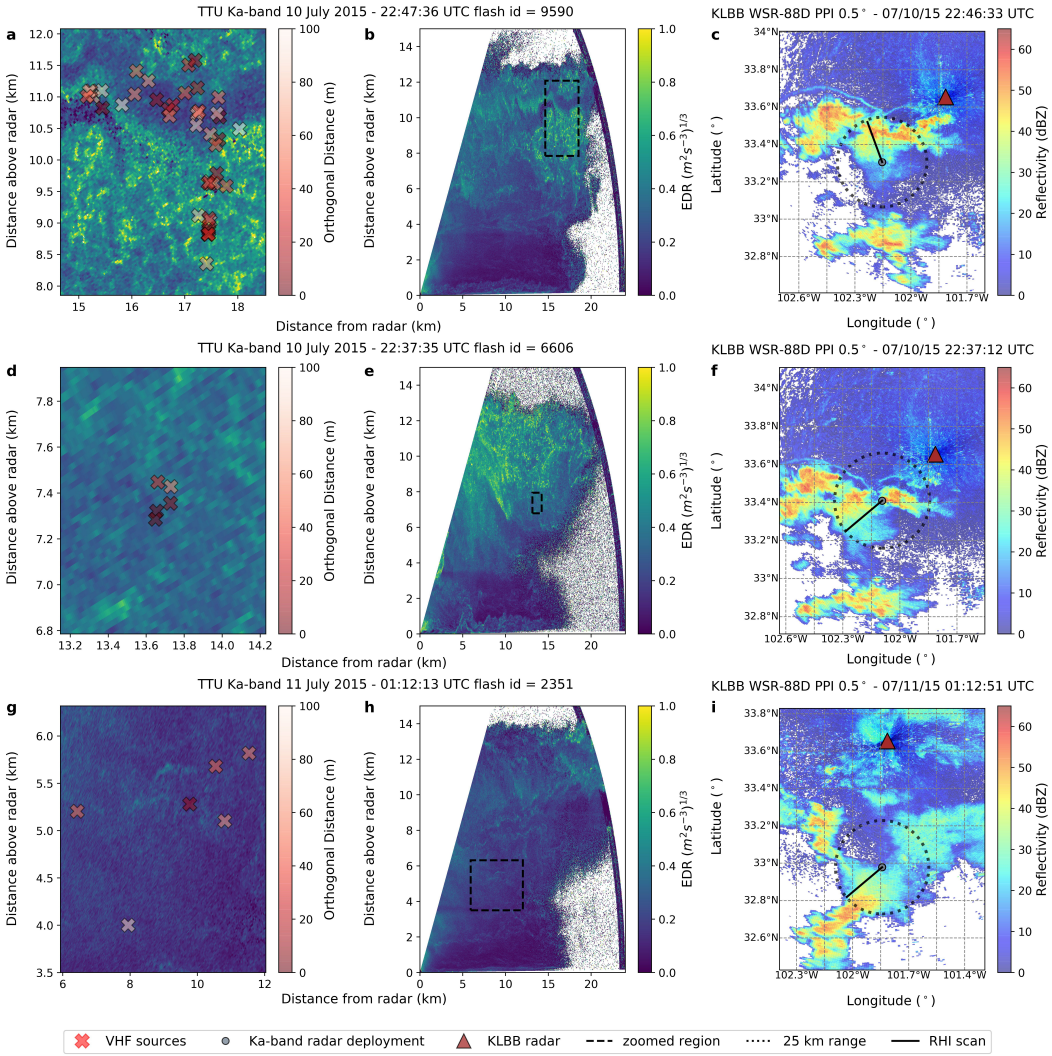

Figure 2. (a),(d),(g) Zoom delimited by the dashed line and (b),(e),(h) overview of $EDR^{0.33}$ from the TTU Ka-band radar RHI scan with VHF sources within 100 m on 10 July 2015 at (a),(b) 22:46:27 UTC and (d),(e) 22:37:35 UTC and (g),(h) on 11 July 2015 at 01:12:13 UTC. PPI 0.5° of Reflectivity (dBZ) from KLBB WSR-88D closest in time to the RHI scan for (c) 22:46:33, (f) 22:37:12 and (i) 01:12:51 UTC. The black dashed circle limits the TTU Ka-band radar range in 25 km and the black continuous line show the actual RHI scan being considered.

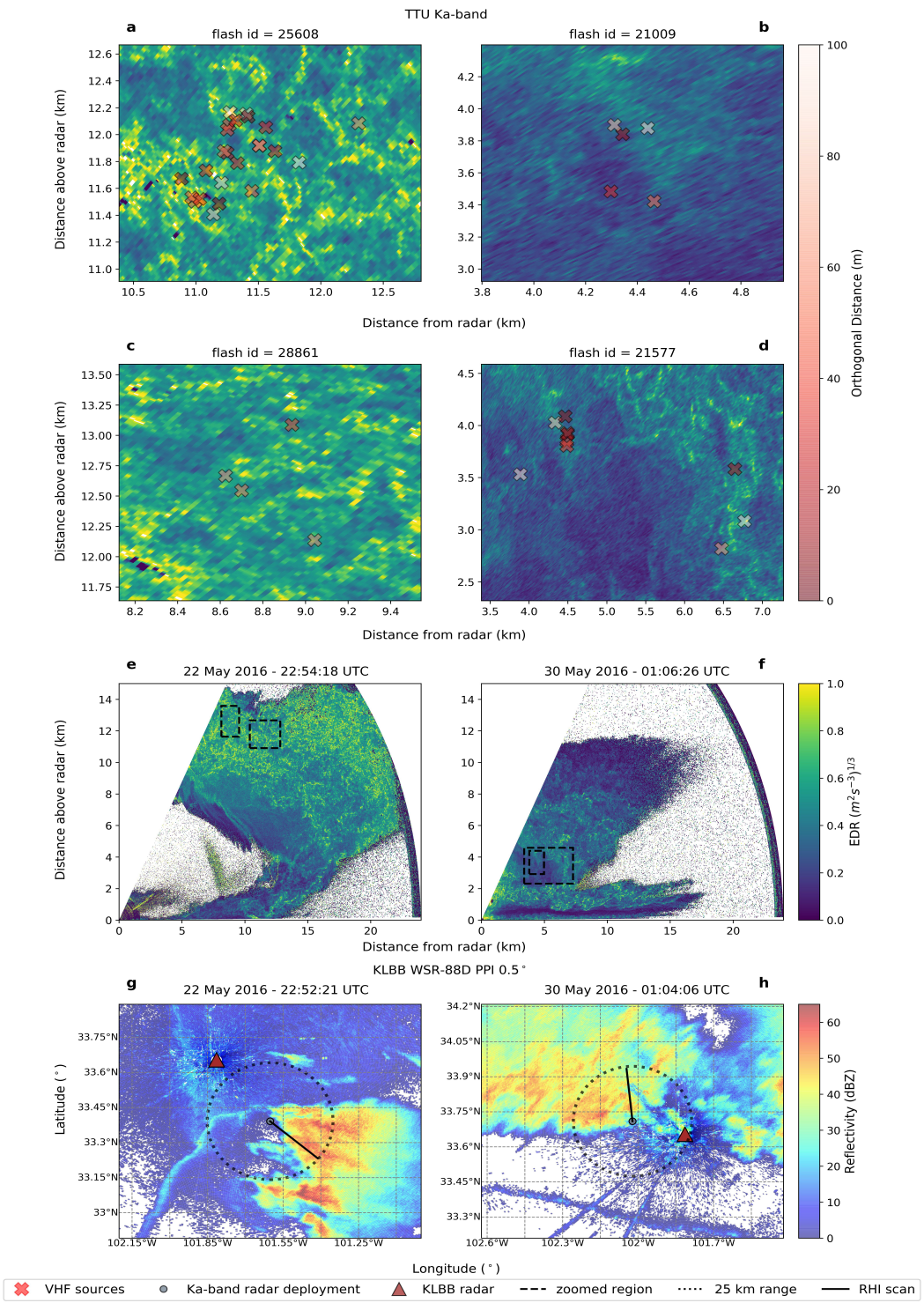

Figure 3. (a),(b),(c),(d) Zoom delimited by the dashed line and (e),(f) overview of $EDR^{0.33}$ from the TTU Ka-band radar RHI scan with VHF sources within 100 m on (a),(c),(e) 22 May 2016 at 22:54:18 UTC and on (b),(d),(f) 30 May 2016 at 01:06:26 UTC. PPI 0.5° of Reflectivity (dBZ) from KLBB WSR-88D closest in time to the RHI scan for (g) 22 May 2016 at 22:52:21 and (h) 30 May 2016 at 01:04:06 UTC. The black dashed circle limits the TTU Ka-band radar range in 25 km and the black continuous line show the actual RHI scan being considered.

The thresholds for turbulence intensity were based on the EDR magnitude. The EDR for a well-developed cumulus cloud is typically around 0.34 $(m^2s^{-3})^{1/3}$ (Pinsky & Khain, 1997), so we adopted this value as upper bound of low turbulence intensity. In thunderstorm measurements by Istok and Doviak (1986), the cumulative probability for EDR exceeded $0.8(m^2s^{-3})^{1/3}$ in 95% and $1(m^2s^{-3})^{1/3}$ in 99% of their analyzed storm's volume. We chose to classify high turbulence regions as those with a threshold above the 95th percentile in our data, which corresponded to $0.77(m^2s^{-3})^{1/3}$, a value consistent with earlier observations.

3.1 Decrease in turbulence intensity as the distance from flash initiation increases

In figure 1(a), there is a region of larger EDR values closer to the flash initiation point in the upper left corner. More production of turbulence means more eddies to dissipate and hence higher EDR values. This turbulent region is associated with more frequent flash initiations as they are predominantly smaller flashes intercepting the scan at higher altitudes (above 10 km) and are distributed over a wide range of high EDR values. In the lower right corner, we have a region of low EDR values farther away from the flash initiation point associated with lower altitude (< 9 km) initiation. This less turbulent region seems to favor flash propagation, since it is permitted across lower EDR values and among larger flash areas. Overall, between these two regions on the plot, we can observe a gradient of flash sizes as EDR decreases and distance from flash initiation increases.

From the RHI perspective, the intercepted spot in the scan changed from being mostly high EDR values at small distances in patchy areas (Figure 2 a - c) to low EDR values in more homogeneous regions at large distances (Figure 2 g - i). As EDR values decreased there was also a decrease in lightning initiation altitude, which is consistent with larger scale, resolved, turbulence dominating around cloud base whereas the small-scale, unresolved, turbulence dominates around cloud top (Fang et al., 2014).

In figure 1(a), there were no flashes below and to the left of the line connecting EDR $= 0.2$ at zero distance and EDR $= 0.0$ at 5 km distance, which may indicate that there is a lower bound on the velocity variability required for flash initiation.

Calhoun et al. (2013) reported a distinct difference in the frequency and size of flashes as the distance from the turbulent updraft core increased, as is also consistent with our results. Lightning that initiated in or near the main updraft in the storm core had a smaller flash area. Lightning in the anvil frequently spanned a greater horizontal extent. In our results, the same gradient from small to large flashes was observed as the distance from flash initiation increased and the EDR value associated with the lightning propagation where it crossed the scan decreased. That pattern parallels how the higher EDR in the updraft decreases when moving towards the anvil.

3.2 High turbulence intensity near flash initiation

The flashes initiating closest to the largest turbulence are worth closer examination. We identified a broad region of high EDR values near the initiation of small flash areas with mean initiation altitude of 11.7 km ($\pm$1.5 km) (Figure 3 a,c,e,g). The RHI scans on figure 3 a,c,e,g showed more finely structured regions of EDR at upper levels consistent with spatial electrical inhomogeneity provided by smaller pockets of charge (Brothers et al., 2018).

The presence of large EDR values in the upper region of thunderstorms has been previously documented via large spectrum width measurements (Istok, 1981; Knupp & Cotton, 1982; Istok & Doviak, 1986). An explanation for the concentration of small flashes in regions of large EDR values in the upper portion of the cloud could be similar to the

lightning behaviour documented by (Calhoun et al., 2014). In their study, an updraft surge produced a charge structure consisting of an upper-level negative charge above 11 km above a mid-level positive charge, with lightning in the main updraft region limited to higher altitudes as in this case. Most flashes were initiated at altitudes between 8 and 11 km and the peak region of flash initiations was near 10 km due to the strong updraft (Calhoun et al., 2014). The majority of the high variability in velocity for small flashes comes from events with similar properties (Figure 3 a,c,e,g) in our data.

Our observations of more turbulence and lightning at higher levels are consistent with the presence of strong updraft producing the turbulence. Regions of higher vertical velocity variability observed with radar appear to be near the cloud top where entrainment processes are most active (Kollias et al., 2001). The folding process by adjacent turbulent eddies can move charge from screening layers into the cloud. The repetition of this process and the resultant deformation can increase locally and instantaneously the charge density (Colgate, 1967). Any lightning activity close to the upper cloud boundary could indicate an interaction of the screening layer charge with the charge produced and advected by the updraft (Calhoun et al., 2013). However, deeper in the storm it is more likely that microphysically generated net storm charge is being folded, as would be necessary to explain the small flashes in the lightning bubbles observed by Yoshida et al. (2017).

In narrow areas between updrafts and downdrafts, the spectrum width increases substantially due to high values of vertical velocity shear across the horizontal dimension. This transition is sharp and can occur within the narrow horizontal dimension of the radar beam and during the short sampling period as the cloud advects through the radar sampling volume (Kollias et al., 2001). In Kollias et al. (2001), the highest spectrum widths were observed along the updraft–downdraft interfaces, where the broadening of the spectra was suggested to be due to sharp horizontal gradients in the vertical wind or turbulence generated by this shear. Fang et al. (2014) also identified high EDR values on the top and edges of the updraft surrounding lower EDR areas. However, it was suggested that the larger EDR values at the edges of the updraft were due to the horizontal shear of the vertical wind instead of turbulence. The boundaries of strong updrafts and downdrafts were associated with large values of the variance in Battan (1980).

The explanation that shear is a large contributor to the final spectrum width value requires that some of the largest EDR values are due to anisotropic eddies. Also, eddies are limited by the upper boundary of the cloud, which introduces anisotropy that could have led to the presence of small pockets of high EDR. In this case, the EDR estimate would happen at the energy-containing range instead of happening at the inertial range. So, high EDR values would be an overestimation of EDR due to inclusion of variance from eddy sizes that do not fit our assumptions. In such cases, the spectrum-width-derived EDR can be larger than the constant EDR we expect in the inertial range. Regardless, the presence of higher velocity variability by any mechanism is consistent with the idea that motions of charged hydrometeors are more complex and less layered.

Lightning flashes propagated up to 10 km through highly turbulent regions (high EDR values and velocity gradient magnitude) in a few cases (Figure 1), though as the distance from initiation increases, the flashes are larger and at lower altitudes. These flashes may be propagating through TKE produced by the updraft and advected downwind while it cascades to smaller (inertial range) scales.

The methodology and analysis do not assume anything about the distribution of turbulence intensity between the flash initiation point and the interception location on the RHI scan. However, the absence of points in the upper right portion of figure 1 (a) indicates that high EDR values also appear to limit the propagation of lightning flashes beyond a certain distance. As propagation distance increases, the maximum allowed EDR decreases as lower altitude initiations are observed.

3.3 Low turbulence intensity near flash initiation

Low EDR values and velocity variability at small distances were found to be associated with small and medium flash areas and lower altitude initiation (Figure 1). The flashes selected propagated through regions where less turbulent energy was being dissipated in proximity to the flash initiation points, as seen by less variability and smaller magnitudes of EDR along and across the radar beams (Figure 3 b,d,f,h).

Kollias et al. (2001) found low spectrum widths in the updraft interior for fair-weather cumulus clouds with updrafts of $5.5 - 6.0\,m\,s^{-1}$, where a less turbulent flow was associated with relatively small horizontal variability of vertical air motions and a gradual accelerating motion in the vertical. Fang et al. (2014) also observed a region of low EDR values in the updraft core associated with a more laminar flow in continental stratocumulus clouds.

The unmixed updraft core is less affected by wind shear or droplet size distribution broadening. Thus, the spectrum width in the unmixed updraft is mainly due to turbulence (Kollias et al., 2001). Even though these studies are for non-precipitating clouds, their results explain our observations we infer to be in the inner lower part of the updraft region. A common observation through many studies was that the intensity of turbulence increases with height in the cloud (Knupp & Cotton, 1982; Istok & Doviak, 1986)

Since stratiform regions are associated with less turbulence and smaller vertical velocities, flash initiation in those regions that produce positive polarity ground strikes (Lang et al., 2004) would also be expected in this category — a topic worth investigation in future studies.

4 Concluding Remarks

To improve lightning predictability in storms, it is important to recognize and understand the effect of thunderstorm kinematics on lightning initiation and propagation, including any characteristics that vary as a function of the flash size scale. To include the smallest flashes, we analyzed the electrical and kinematic connection at scales within the thunderstorm's inertial range.

By assessing the kinematic properties of regions through which lightning propagated, and the distance to each flash's initiation, the observations confirmed our hypothesis that, for the majority of the flashes during the radar sampling, greater turbulence intensity was correlated with smaller distance from initiation of smaller flashes. As the distance from flash initiation increased, moving away from the regions where the input of kinetic energy leading to turbulence was happening (i.e., the updraft), there was a gradient toward less turbulent regions favoring propagation of larger flashes.

Furthermore, the analysis distinguished other turbulence-lightning relationships in specific regions of the storm. The classification based on EDR assigned to a particular observation what storm structures led to the observed EDR pattern. In the regions we inferred as updraft regions, we identified two contrasting behaviors.

First, flashes initiated at lower altitudes were in regions of smaller EDR values. These locations are plausible within the lower, inner part of updrafts that are associated with unmixed flow and hence present low EDR values. This category included small- and medium-sized flashes from the dataset. The absence of flashes initiating nearby at low EDR values suggests there may be a lower bound on turbulence intensity for lightning initiation.

Second, smaller flashes initiated at higher altitudes in the cloud in high EDR values. Upper regions of the cloud have the strongest updrafts, consistent with high EDR values due to energetic small scale variability associated with a great input of energy,

entrainment, and the sharp transition to downdraft. Such conditions are favorable to a concentration of small flashes at high altitudes.

Finally, the lack of flash propagation through highly turbulent regions suggests a range of turbulence intensity permitted for lightning propagation that varies with distance from its initiation location. There appears to be an upper bound on the allowable turbulence that permits propagation, with that upper bound decreasing with propagation distance.

These data are further evidence that there is a strong coupling between hydrometeor transport on the scale of turbulent eddies in thunderstorms, and the distribution of the electrostatic conditions associated with lightning initiation and propagation.

Acknowledgments

This study was supported by the National Science Foundation Award AGS-1352144 under the CAREER Program. Mr. Jerry Guynes capably maintained the TTU-Ka radars. Data collection would not have been possible without the commitment of a large group of faculty, graduate students and research staff at Texas Tech University, for whom we are grateful. Dr. Vanna Chmielewski, Dr. Vicente Salinas and Ms. Samantha Berkseth played especially crucial roles in LMA and radar data collection and post-processing. The code (Souza & Bruning, 2021) for reproducing the results of this study, and the TTU Ka-band radar (Bruning, Berkseth, et al., 2021) and WTLMA (Bruning, Chmielewski, et al., 2021) data used can be accessed at the Zenodo public repository using the DOIs associated with the dataset citations above. The WSR-88D data is available on National Climatic Data Center (NCDC) at `https://www.ncdc.noaa.gov/nexradinv/` setting the location for KLBB (Lubbock, Texas) under level-II base data for the storm days in Supporting information Table S1.

References

Battan, L. J. (1980, May). Observations of two colorado thunderstorms by means of a zenith-pointing doppler radar. *Journal of Applied Meteorology*, *19*(5), 580–592. Retrieved from `https://doi.org/10.1175/1520-0450(1980)019<0580:ootctb>2.0.co;2` doi: 10.1175/1520-0450(1980)019⟨0580:ootctb⟩2.0.co;2

Brothers, M. D., Bruning, E. C., & Mansell, E. R. (2018, August). Investigating the relative contributions of charge deposition and turbulence in organizing charge within a thunderstorm. *Journal of the Atmospheric Sciences*, *75*(9), 3265–3284. Retrieved from `https://doi.org/10.1175/jas-d-18-0007.1` doi: 10.1175/jas-d-18-0007.1

Bruning, E. C., Berkseth, S., Souza, J. C. S., Chmielewski, V. C., & Salinas, V. (2021). *TTU-Ka Mobile Doppler Radar - KTaL 2015-2016.* Dataset. doi: 10.5281/zenodo.4515064

Bruning, E. C., Chmielewski, V. C., Salinas, V., Souza, J. C. S., & Berkseth, S. (2021). *West Texas Lightning Mapping Array - KTaL 2015-2016.* Dataset. doi: 10.5281/zenodo.4509546

Bruning, E. C., & MacGorman, D. R. (2013, November). Theory and observations of controls on lightning flash size spectra. *Journal of the Atmospheric Sciences*, *70*(12), 4012–4029. Retrieved from `https://doi.org/10.1175/jas-d-12-0289.1` doi: 10.1175/jas-d-12-0289.1

Bruning, E. C., Rust, W. D., MacGorman, D. R., Biggerstaff, M. I., & Schuur, T. J. (2010, October). Formation of charge structures in a supercell. *Monthly Weather Review*, *138*(10), 3740–3761. Retrieved from `https://doi.org/10.1175/2010mwr3160.1` doi: 10.1175/2010mwr3160.1

Bryan, G. H., Wyngaard, J. C., & Fritsch, J. M. (2003, 10). Resolution require-

ments for the simulation of deep moist convection. *Monthly Weather Review*, *131*(10), 2394–2416.

Calhoun, K. M., MacGorman, D. R., Ziegler, C. L., & Biggerstaff, M. I. (2013, July). Evolution of lightning activity and storm charge relative to dual-doppler analysis of a high-precipitation supercell storm. *Monthly Weather Review*, *141*(7), 2199–2223. Retrieved from `https://doi.org/10.1175/mwr-d-12-00258.1` doi: 10.1175/mwr-d-12-00258.1

Calhoun, K. M., Mansell, E. R., MacGorman, D. R., & Dowell, D. C. (2014, October). Numerical simulations of lightning and storm charge of the 29–30 may 2004 geary, oklahoma, supercell thunderstorm using EnKF mobile radar data assimilation. *Monthly Weather Review*, *142*(11), 3977–3997. Retrieved from `https://doi.org/10.1175/mwr-d-13-00403.1` doi: 10.1175/mwr-d-13-00403.1

Chmielewski, V. C., & Bruning, E. C. (2016, July). Lightning mapping array flash detection performance with variable receiver thresholds. *Journal of Geophysical Research: Atmospheres*, *121*(14), 8600–8614. Retrieved from `https://doi.org/10.1002/2016jd025159` doi: 10.1002/2016jd025159

Colgate, S. A. (1967, January). Enhanced drop coalescence by electric fields in equilibrium with turbulence. *Journal of Geophysical Research*, *72*(2), 479–487. Retrieved from `https://doi.org/10.1029/jz072i002p00479` doi: 10.1029/jz072i002p00479

Crum, T. D., & Alberty, R. L. (1993, September). The WSR-88d and the WSR-88d operational support facility. *Bulletin of the American Meteorological Society*, *74*(9), 1669–1687. Retrieved from `https://doi.org/10.1175/1520-0477(1993)074<1669:twatwo>2.0.co;2` doi: 10.1175/1520-0477(1993)074⟨1669:twatwo⟩2.0.co;2

Deierling, W., & Petersen, W. A. (2008, August). Total lightning activity as an indicator of updraft characteristics. *Journal of Geophysical Research*, *113*(D16). Retrieved from `https://doi.org/10.1029/2007jd009598` doi: 10.1029/2007jd009598

Devenish, B. J., Bartello, P., Brenguier, J.-L., Collins, L. R., Grabowski, W. W., IJzermans, R. H. A., ... Warhaft, Z. (2012, February). Droplet growth in warm turbulent clouds. *Quarterly Journal of the Royal Meteorological Society*, *138*(667), 1401–1429. Retrieved from `https://doi.org/10.1002/qj.1897` doi: 10.1002/qj.1897

Edens, H. E., Eack, K. B., Rison, W., & Hunyady, S. J. (2014, February). Photographic observations of streamers and steps in a cloud-to-air negative leader. *Geophysical Research Letters*, *41*(4), 1336–1342. Retrieved from `https://doi.org/10.1002/2013gl059180` doi: 10.1002/2013gl059180

Fang, M., Albrecht, B. A., Ghate, V. P., & Kollias, P. (2014). Turbulence in continental stratocumulus, part ii: Eddy dissipation rates and large-eddy coherent structures. *Boundary-layer meteorology*, *150*(3), 361–380.

Fuchs, B. R., Rutledge, S. A., Bruning, E. C., Pierce, J. R., Kodros, J. K., Lang, T. J., ... Rison, W. (2015, July). Environmental controls on storm intensity and charge structure in multiple regions of the continental united states. *Journal of Geophysical Research: Atmospheres*, *120*(13), 6575–6596. Retrieved from `https://doi.org/10.1002/2015jd023271` doi: 10.1002/2015jd023271

Helmus, J. J., & Collis, S. M. (2016, July). The python ARM radar toolkit (py-ART), a library for working with weather radar data in the python programming language. *Journal of Open Research Software*, *4*. Retrieved from `https://doi.org/10.5334/jors.119` doi: 10.5334/jors.119

Hernandez-Deckers, D., & Sherwood, S. C. (2016, September). A numerical investigation of cumulus thermals. *Journal of the Atmospheric Sciences*, *73*(10), 4117–4136. Retrieved from `https://doi.org/10.1175/jas-d-15-0385.1` doi: 10.1175/jas-d-15-0385.1

Hirth, B. D., Schroeder, J. L., Gunter, W. S., & Guynes, J. G. (2012, June). Measuring a utility-scale turbine wake using the TTUKa mobile research radars. *Journal of Atmospheric and Oceanic Technology*, *29*(6), 765–771. Retrieved from https://doi.org/10.1175/jtech-d-12-00039.1 doi: 10.1175/jtech-d-12-00039.1

Istok, M. (1981). Analysis of doppler spectrum broadening mechanisms in thunderstorms. In *Conference on radar meteorology, 20 th, boston, ma* (pp. 454–458).

Istok, M., & Doviak, R. (1986, October). Analysis of the relation between doppler spectral width and thunderstorm turbulence. *Journal of the Atmospheric Sciences*, *43*(20), 2199–2214. Retrieved from https://doi.org/10.1175/1520-0469(1986)043<2199:aotrbd>2.0.co;2 doi: 10.1175/1520-0469(1986)043⟨2199:aotrbd⟩2.0.co;2

Knupp, K. R., & Cotton, W. R. (1982). An intense, quasi-steady thunderstorm over mountainous terrain. part iii: Doppler radar observations of the turbulent structure. *Journal of the Atmospheric Sciences*, *39*(2), 359–368.

Kollias, P., Albrecht, B., Lhermitte, R., & Savtchenko, A. (2001). Radar observations of updrafts, downdrafts, and turbulence in fair-weather cumuli. *Journal of the atmospheric sciences*, *58*(13), 1750–1766.

Kolmogorov, A. N. (1941). The local structure of turbulence in incompressible viscous fluid for very large reynolds numbers. *Dokl. ANSSSR*, *30*, 301–305.

Kostinskiy, A. Y., Marshall, T. C., & Stolzenburg, M. (2020, November). The mechanism of the origin and development of lightning from initiating event to initial breakdown pulses (v.2). *Journal of Geophysical Research: Atmospheres*, *125*(22). Retrieved from https://doi.org/10.1029/2020jd033191 doi: 10.1029/2020jd033191

Lang, T., & Guy, N. (2017). Diagnosing turbulence for research aircraft safety using open source toolkits. *Results in Physics*, *7*, 2425–2426. Retrieved from https://doi.org/10.1016/j.rinp.2017.07.015 doi: 10.1016/j.rinp.2017.07.015

Lang, T., Rutledge, S., & Wiens, K. (2004, May). Origins of positive cloud-to-ground lightning flashes in the stratiform region of a mesoscale convective system. *Geophysical Research Letters*, *31*(10), n/a–n/a. Retrieved from https://doi.org/10.1029/2004gl019823 doi: 10.1029/2004gl019823

Lund, N. R., MacGorman, D. R., Schuur, T. J., Biggerstaff, M. I., & Rust, W. D. (2009, December). Relationships between lightning location and polarimetric radar signatures in a small mesoscale convective system. *Monthly Weather Review*, *137*(12), 4151–4170. Retrieved from https://doi.org/10.1175/2009mwr2860.1 doi: 10.1175/2009mwr2860.1

Mareev, E. A., & Dementyeva, S. O. (2017, July). The role of turbulence in thunderstorm, snowstorm, and dust storm electrification. *Journal of Geophysical Research: Atmospheres*, *122*(13), 6976–6988. Retrieved from https://doi.org/10.1002/2016jd026150 doi: 10.1002/2016jd026150

Marshall, T. (2005). Observed electric fields associated with lightning initiation. *Geophysical Research Letters*, *32*(3). Retrieved from https://doi.org/10.1029/2004gl021802 doi: 10.1029/2004gl021802

Pinsky, M., & Khain, A. (1997, October). Turbulence effects on droplet growth and size distribution in clouds—a review. *Journal of Aerosol Science*, *28*(7), 1177–1214. Retrieved from https://doi.org/10.1016/s0021-8502(97)00005-0 doi: 10.1016/s0021-8502(97)00005-0

Rison, W., Thomas, R. J., Krehbiel, P. R., Hamlin, T., & Harlin, J. (1999). A gps-based three-dimensional lightning mapping system: Initial observations in central new mexico. *Geophysical Research Letters*, *26*(23), 3573–3576.

Saunders, C. P. R. (2008, April). Charge separation mechanisms in clouds. *Space Science Reviews*, *137*(1-4), 335–353. Retrieved from https://doi.org/10.1007/s11214-008-9345-0 doi: 10.1007/s11214-008-9345-0

Saunders, C. P. R., & Brooks, I. M. (1992). The effects of high liquid water content on thunderstorm charging. *Journal of Geophysical Research*, *97*(D13), 14671. Retrieved from https://doi.org/10.1029/92jd01186 doi: 10.1029/92jd01186

Souza, J. C. S., & Bruning, E. C. (2021). *LMAinterceptRHI.* Dataset. doi: 10.5281/zenodo.4531657

Stolzenburg, M., Rust, W. D., & Marshall, T. C. (1998, June). Electrical structure in thunderstorm convective regions: 3. synthesis. *Journal of Geophysical Research: Atmospheres*, *103*(D12), 14097–14108. Retrieved from https://doi.org/10.1029/97jd03545 doi: 10.1029/97jd03545

Takahashi, T. (1978, August). Riming electrification as a charge generation mechanism in thunderstorms. *Journal of the Atmospheric Sciences*, *35*(8), 1536–1548. Retrieved from https://doi.org/10.1175/1520-0469(1978)035<1536:reaacg>2.0.co;2 doi: 10.1175/1520-0469(1978)035⟨1536:reaacg⟩2.0.co;2

Takahashi, T., & Miyawaki, K. (2002, March). Reexamination of riming electrification in a wind tunnel. *Journal of the Atmospheric Sciences*, *59*(5), 1018–1025. Retrieved from https://doi.org/10.1175/1520-0469(2002)059<1018:roreia>2.0.co;2 doi: 10.1175/1520-0469(2002)059⟨1018:roreia⟩2.0.co;2

Thomas, R. J. (2004). Accuracy of the lightning mapping array. *Journal of Geophysical Research*, *109*(D14). Retrieved from https://doi.org/10.1029/2004jd004549 doi: 10.1029/2004jd004549

Williams, Cornman, L., Yee, J., Carson, S., Blackburn, G., & Craig, J. (2006, January). NEXRAD detection of hazardous turbulence. In *44th AIAA aerospace sciences meeting and exhibit.* American Institute of Aeronautics and Astronautics. Retrieved from https://doi.org/10.2514/6.2006-76 doi: 10.2514/6.2006-76

Williams, Weber, M. E., & Orville, R. E. (1989). The relationship between lightning type and convective state of thunderclouds. *Journal of Geophysical Research*, *94*(D11), 13213. Retrieved from https://doi.org/10.1029/jd094id11p13213 doi: 10.1029/jd094id11p13213

Yoshida, S., Adachi, T., Kusunoki, K., Hayashi, S., Wu, T., Ushio, T., & Yoshikawa, E. (2017, April). Relationship between thunderstorm electrification and storm kinetics revealed by phased array weather radar. *Journal of Geophysical Research: Atmospheres*, *122*(7), 3821–3836. Retrieved from https://doi.org/10.1002/2016jd025947 doi: 10.1002/2016jd025947

Supporting Information for Observations of the influence of turbulence on lightning initiation and propagation

Jessica C. S. Souza[1], Eric C. Bruning[1]

[1]Department of Geosciences, Atmospheric Science Group, Texas Tech University, Lubbock, Texas, USA

Contents of this file

1. Figure S1
2. Table S1

Introduction

The following contains supporting information for the storms analyzed in the study (Table S1). The data sets collected considered the period when the storms were within the observational domain (Figure S1).

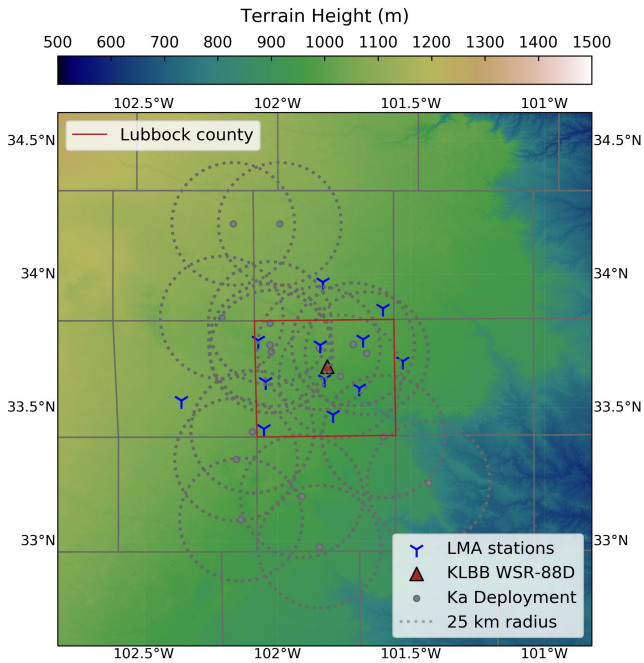

Figure S1. Spatial distribution of the WTLMA stations, KLBB WSR-88D, TTU Ka-band radar deployments and their radius of data acquisition across the South Plains during the KTaL experiment. Lubbock county is highlighted in red.

Table S1. Summary of the storms analyzed.

Date	Interval Considered* (UTC)	Predominant Storm Mode	Life Cycle Stage
29-30 June 2015	22:23 - 00:23	Squall Line	Mature - Decaying
04 July 2015	05:30 - 05:50	MCS	Decaying
06-07 July 2015	22:27 - 23:08 22:44 - 01:22	Multicell - MCS	Mature
10-11 July 2015	22:26 - 22:52 01:00 - 01:12 02:20 - 02:51	Multicell	Mature Mature Mature - Decaying
19 May 2016	04:17 - 04:26	Multicell	Mature
22 May 2016	22:38 - 00:36	Multicell	Developing - Mature - Decaying
30 May 2016	00:26 - 01:48	Multicell - MCS	Mature - Decaying
01 June 2016	02:21 - 03:10	Multicell	Decaying
15 June 2016	23:26 - 23:57	Multicell	Mature